Understanding light trapping by resonant coupling to guided modes and the importance of the mode profile

Fiona J. Beck,[1,3,5] Alexandros Stavrinadis,[1] Tania Lasanta,[1] John-Paul Szczepanick,[2] and Gerasimos Konstantatos[1,4]

[1]*ICFO - Institut de Ciències Fotòniques, The Barcelona Institute of Science and Technology, Castelldefels, Barcelona, 08860, Spain*
[2]*On Sun Systems, Av. Carl Friedrich Gauss, Mediterranean Technology Park, Castelldefels, Barcelona, 08860, Spain*
[3]*Currently with the Research School of Engineering, College of Engineering and Computer Science, The Australian National University, Acton, Canberra, 0200, Australia*
[4]*ICREA - Institució Catalana de Recerca i Estudis Avançats, 08010 Barcelona, Spain*
[5]*gerasimos.konstantatos@icfo.es*
[6]*fiona.beck@anu.edu.au*

Abstract: We present a simple conceptual model describing the absorption enhancement provided by diffraction gratings due to resonant coupling to guided modes in a multi-layered structure. In doing so, we provide insight into why certain guided modes are more strongly excited than others and demonstrate that the spatial overlap of the mode profile with the grating is important. The model is verified by comparison to optical simulations and experimental measurements. We fabricate metal nanoparticle gratings integrated as back contacts in solution-processed PbS colloidal quantum dot photodiodes. The measured photocurrent at the target wavelength is enhanced by 250%, with reference to planar devices, due to resonant coupling to guided modes with strong spatial overlap with the gratings. In comparison, resonant coupling to weakly overlapping modes results in a 25% increase at the same wavelength.

OCIS codes: (250.0250) Optoelectronics; (050.6624) Subwavelength structures.

References and links

1. V. E. Ferry, M. A. Verschuuren, H. B. T. Li, E. Verhagen, R. J. Walters, R. E. I. Schropp, H. A. Atwater, and A. Polman, "Light trapping in ultrathin plasmonic solar cells," Opt. Express **18**(S2 Suppl 2), A237–A245 (2010).
2. A. Mihi, F. J. Beck, T. Lasanta, A. K. Rath, and G. Konstantatos, "Imprinted electrodes for enhanced light trapping in solution processed solar cells," Adv. Mater. **26**(3), 443–448 (2014).
3. A. Ono, Y. Enomoto, Y. Matsumura, H. Satoh, and H. Inokawa, "Broadband absorption enhancement of thin SOI photodiode with high-density gold nanoparticles," Opt. Express **2329**, 5663–5666 (2014).
4. F. J. Beck, A. Stavrinadis, S. L. Diedenhofen, T. Lasanta, and G. Konstantatos, "Surface plasmon polariton couplers for light trapping in thin-film absorbers and their application to colloidal quantum dot optoelectronics," ACS Photonics **1**(11), 1197–1205 (2014).
5. M. Dragoman and D. Dragoman, "Plasmonics: applications to nanoscale terahertz and optical devices," Prog. Quantum Electron. **32**(1), 1–41 (2008).
6. G. Sun, J. B. Khurgin, and R. A. Soref, "Plasmonic light-emission enhancement with isolated metal nanoparticles and their coupled arrays," J. Opt. Soc. Am. B **25**(10), 1748 (2008).
7. S. Mokkapati and K. R. Catchpole, "Nanophotonic light trapping in solar cells," J. Appl. Phys. **112**(10), 101101 (2012).
8. S. A. Maier, M. L. Brongersma, P. G. Kik, S. Meltzer, A. A. G. Requicha, and H. A. Atwater, "Plasmonics - a route to nanoscale optical devices," Adv. Mater. **13**(19), 1501–1505 (2001).
9. E. Yablonovitch and G. D. Cody, "Intensity enhancement in textured optical sheets for solar-cells," IEEE Trans. Electron. Dev. **29**(2), 300–305 (1982).
10. H. R. Stuart and D. G. Hall, "Thermodynamic limit to light trapping in thin planar structures," J. Opt. Soc. Am. A **14**(11), 3001 (1997).
11. Z. Yu, A. Raman, and S. Fan, "Fundamental limit of nanophotonic light trapping in solar cells," Proc. Natl. Acad. Sci. U.S.A. **107**(41), 17491–17496 (2010).

#253156 Received 3 Nov 2015; revised 23 Dec 2015; accepted 3 Jan 2016; published 11 Jan 2016

12. J. N. Munday, D. M. Callahan, and H. A. Atwater, "Light trapping beyond the 4n2 limit in thin waveguides," Appl. Phys. Lett. **100**(12), 121121 (2012).
13. P. Bermel, C. Luo, L. Zeng, L. C. Kimerling, and J. D. Joannopoulos, "Improving thin-film crystalline silicon solar cell efficiencies with photonic crystals," Opt. Express **15**(25), 16986–17000 (2007).
14. C. Rockstuhl, S. Fahr, K. Bittkau, T. Beckers, R. Carius, F. J. Haug, T. Söderström, C. Ballif, and F. Lederer, "Comparison and optimization of randomly textured surfaces in thin-film solar cells," Opt. Express **18**(S3 Suppl 3), A335–A341 (2010).
15. R. A. Pala, J. S. Q. Liu, E. S. Barnard, D. Askarov, E. C. Garnett, S. Fan, and M. L. Brongersma, "Optimization of non-periodic plasmonic light-trapping layers for thin-film solar cells," Nat. Commun. **4**, 2095 (2013).
16. M.-C. van Lare and A. Polman, "Optimized scattering power spectral density of photovoltaic light trapping patterns," ACS Photonics **2**, 822–831 (2015).
17. E. R. Martins, J. Li, Y. Liu, V. Depauw, Z. Chen, J. Zhou, and T. F. Krauss, "Deterministic quasi-random nanostructures for photon control," Nat. Commun. **4**, 2665 (2013).
18. F. J. Haug, T. Söderström, O. Cubero, V. Terrazzoni-Daudrix, and C. Ballif, "Influence of the ZnO buffer on the guided mode structure in Si/ZnO/Ag multilayers," J. Appl. Phys. **106**(4), 044502 (2009).
19. F. J. Haug, K. Söderström, A. Naqavi, and C. Ballif, "Resonances and absorption enhancement in thin film silicon solar cells with periodic interface texture," J. Appl. Phys. **109**(8), 084516 (2011).
20. N. N. Lal, H. Zhou, M. Hawkeye, J. K. Sinha, P. N. Bartlett, G. A. J. Amaratunga, and J. J. Baumberg, "Using spacer layers to control metal and semiconductor absorption in ultrathin solar cells with plasmonic substrates," Phys. Rev. B – Condens. Matter Mater. Phys. **85**(24), 1–10 (2012).
21. S. A. McDonald, G. Konstantatos, S. Zhang, P. W. Cyr, E. J. D. Klem, L. Levina, and E. H. Sargent, "Solution-processed PbS quantum dot infrared photodetectors and photovoltaics," Nat. Mater. **4**(2), 138–142 (2005).
22. J. Tang and E. H. Sargent, "Infrared colloidal quantum dots for photovoltaics: fundamentals and recent progress," Adv. Mater. **23**(1), 12–29 (2011).
23. D. V. Talapin, J.-S. Lee, M. V. Kovalenko, and E. V. Shevchenko, "Prospects of colloidal nanocrystals for electronic and optoelectronic applications," Chem. Rev. **110**(1), 389–458 (2010).
24. M. M. Adachi, A. J. Labelle, S. M. Thon, X. Lan, S. Hoogland, and E. H. Sargent, "Broadband solar absorption enhancement via periodic nanostructuring of electrodes," Sci. Rep. **3**, 2928 (2013).
25. F. P. García de Arquer, F. J. Beck, and G. Konstantatos, "Absorption enhancement in solution processed metal-semiconductor nanocomposites," Opt. Express **19**(21), 21038–21049 (2011).
26. F. P. García de Arquer, F. J. Beck, M. M. Bernechea, and G. Konstantatos, "Plasmonic light trapping leads to responsivity increase in colloidal quantum dot photodetectors," Appl. Phys. Lett. **100**(4), 043101 (2012).
27. U. W. Paetzold, E. Moulin, B. E. Pieters, R. Carius, and U. Rau, "Design of nanostructured plasmonic back contacts for thin-film silicon solar cells," Opt. Express **19**(S6 Suppl 6), A1219–A1230 (2011).
28. U. W. Paetzold, E. Moulin, D. Michaelis, W. Böttler, C. Wächter, V. Hagemann, M. Meier, R. Carius, and U. Rau, "Plasmonic reflection grating back contacts for microcrystalline silicon solar cells," Appl. Phys. Lett. **99**(18), 94–96 (2011).
29. S. Mokkapati, F. J. Beck, A. Polman, and K. R. Catchpole, "Designing periodic arrays of metal nanoparticles for light-trapping applications in solar cells," Appl. Phys. Lett. **95**(5), 053115 (2009).
30. Lumerical FDTD Solutions, version 6.0.3, *www.lumerical.com*, (Lumerical Solutions Inc. 2008), Vancouver.
31. P. B. Johnson and R. W. Christy, "Optical Constants of the Noble Metals," Phys. Rev. B **6**(12), 4370–4379 (1972).
32. K. R. Catchpole and A. Polman, "Design principles for particle plasmon enhanced solar cells," Appl. Phys. Lett. **93**(19), 191113 (2008).
33. M. Mariano, F. J. Rodríguez, P. Romero-Gomez, G. Kozyreff, and J. Martorell, "Light coupling into the whispering gallery modes of a fiber array solar cell for mechanically fixed sun tracking," (in preparation).
34. B. R. Hyun, J. J. Choi, K. L. Seyler, T. Hanrath, and F. W. Wise, "Heterojunction PbS nanocrystal solar cells with oxide charge-transport layers," ACS Nano **7**(12), 10938–10947 (2013).

1. Introduction

Light management in thin film absorbers and optoelectronic devices can lead to significant enhancements in device performance. There are numerous examples in literature of successful implementation of light trapping in solar cells [1,2], photodiodes [3,4], sensors [5], and LEDs [6]. In particular, nano-photonic schemes – wavelength scale photonic structures resulting in diffraction, excitation of optical resonances, and enhanced optical fields – are increasingly interesting as optoelectronic devices get smaller and thinner [7,8].

However it is achieved, the goal of light trapping is to maximize light absorption. For a weakly absorbing, optically thick substrate in air, with a photonic mode density dependent on the refractive index, n, full randomization of light leads to an absorption enhancement of $4n^2$: the so called Lambertian or bulk limit [9]. Optically thin absorbers support discrete guided modes, with a photonic mode density that is dependent on the thickness and material

#253156 Received 3 Nov 2015; revised 23 Dec 2015; accepted 3 Jan 2016; published 11 Jan 2016

properties of the film. In this case, the estimation of the upper limit for light trapping is somewhat more complex. Stuart and Hall showed that in general the maximum enhancement is reduced as the number of available guided modes decreased [10]. More recently, Yu et al. employed statistical coupled mode theory to demonstrate that the bulk limit can be reached and even exceeded in particular cases: where only one mode is supported by the film and is confined in a deep subwavelength volume [11]. A similar conclusion was reached by Munday who showed that guided modes with low group velocity, as compared to propagating modes in the system, can provide enhancements beyond the Lambertian limit [12].

To approach these theoretical maxima, the mechanism for coupling light to these modes needs to be considered. Periodic structures can couple diffracted light into specific modes within a narrow wavelength range [13]. Conversely, random structures permit coupling of incoherently scattered light to a range of modes over a large spectral region [14]. Both strategies have been employed to provide light trapping in thin absorbing layers and a nice comparison can be found in [1]. More recently, several groups have demonstrated methods of designing quasi-random scattering geometries, opening up the possibility of targeted coupling to the guided modes in a structure over a given wavelength region [15–17].

However, it is not enough for the coupling condition to be fulfilled; light needs to be efficiently scattered into the guided mode and absorbed in the film. In [15], Pala et al. introduced the concept of a response function, which contained information on how much light was scattered by the nanostructures and absorbed in the material, calculated from simulations of the geometry under study. In order for absorption enhancement to occur the response function has to be large at the wavelengths where coupling to guided modes occurs.

An elegant approach to increasing the light trapping efficiency of diffractive coupling to modes has been presented by Haug and colleagues [18,19]. In this work, parasitic absorption losses were reduced by modifying the mode structure in the target film. By incorporating buffer layers between the semiconductor and the lossy metal layers in multilayered substrates, the field profile of the guided modes was modified, changing where in the structure light was absorbed [18–20]. However, the authors highlighted the fact that it is still not clear why some modes are more strongly excited than others [19].

Here we describe a framework for understanding light trapping in thin film absorbers with periodic gratings, based on an intuitive understanding of the system. We focus our study on a simple and technologically relevant geometry, with 2D metal nanoparticle gratings integrated as back contacts in thin film devices. A detailed analysis of the absorption enhancement provided by resonant coupling of diffracted light to waveguide modes in a multi-layered film is performed, employing full-field 3D optical simulations and with reference to a simple conceptual model. In doing so, we are able to give some insight into why certain modes are more strongly excited and provide more efficient absorption enhancement. We demonstrate that the spatial overlap of the mode and the nanoparticle grating is important to achieve large absorption enhancements.

We fabricate solution-processed hetero-junction photodiodes, based on PbS colloidal quantum dots to experimentally verify the model and the main results of our analysis. Lead based colloidal quantum dots (CQDs) are an interesting optoelectronic material system as the excitonic peak can be tuned from the visible to the near infra-red, covering a wide spectrum, with potential applications in solar energy harvesting, photo detection, and night vision [21,22]. These materials can be manufactured in the solution phase and spin-cast to form dense, cross-linked, semiconductor films on a variety of substrates, reducing the cost of device fabrication [23].

Colloidal quantum dots absorbers are ideal candidates for the implementation of nano-photonic light trapping. Firstly, absorber layers must be thin (~200 nm) to extract carriers, due to low mobilities and short lifetimes in the material [22]. To achieve high efficiencies it is necessary to enhance the absorption in these very thin structures. Recent work demonstrated significant enhancements by nano-structuring the electrodes of heterojunction PbS CQD solar

#253156 Received 3 Nov 2015; revised 23 Dec 2015; accepted 3 Jan 2016; published 11 Jan 2016

cells [2,24]. Secondly, the refractive index is relatively low (n ~2.3) because of the composite nature of the material [25]. This means that they have favorable material constants to benefit from near-field absorption due to the enhanced fields that exist in the vicinity of plasmonic resonances [4,20], and that typical absorber film thicknesses support few guided modes in the bandwidth of interest [26].

By employing the insights gained from our conceptual model we enhance the measured photocurrent at the exciton peak (at a wavelength of ~1000 nm) up to 250% for optimized coupling between diffracted orders and guided modes, compared with an increase of 25% in the same wavelength region for the non-optimized case. These results demonstrate that knowledge of the mode structure of the device is sufficient to design efficient light trapping structures without the need for computationally expensive simulation sweeps.

2. Conceptual model

A schematic of the system under study is given in Fig. 1(a), showing a multi-layered structure typical of thin film optoelectronic devices, consisting of a thin-film absorbing layer, a transparent front cladding layer and an embedded rear metal nanoparticle (MNP) grating. Ag was chosen as an exemplar plasmonic metal in order to study the best case scenario. While this structure does not represent a realistic high efficiency device configuration, it is sufficiently simple to gain insight into the physical processes occurring, and general enough for those insights to be applicable to a wide range of technologies. The structure is illuminated by a plane wave. On reaching the metal grating, the light is strongly scattered by the metal nanoparticles due to the excitation of localized surface plasmons (LSP). Since the nanoparticles are in a periodic arrangement, the light is scattered into diffraction orders (DO), with propagation angles determined by the periodicity of the grating. If the absorber is thin compared to the wavelength of light in the substrate, light propagates in the film in a discrete set of guided modes (GM), determined by the geometry and optical properties of the multi-layered structure. A guided resonance occurs when incident light is coupled to a guided mode via diffraction by the grating. Light propagating in a given mode will then be re-scattered by the grating or absorbed. The objective of our conceptual model is to separate out the physical processes occurring and understand the effect of each on the overall light trapping efficiency.

Light can couple to a guided mode when the propagation angle of the scattered light is equal to that of the guided wave; this is known as the resonant coupling condition [11,13,15,19]. For a periodic grating, the propagation vector of diffracted light is given by the reciprocal lattice vector of the grating, which for a square lattice of periodicity L, is given by: $G_{[pxpy]} = \frac{2\pi}{L} p_{xy}$, where $p_{xy} = \sqrt{p_x^2 + p_y^2}$, and $p_x, p_y = 0,1,2,\ldots$

The propagation vectors, $\beta_{m,}$ of the guided modes in the thin absorber can be obtained approximately from the dispersion relations of the planar multi-layered structure. The dispersion relations were calculated using the transfer matrix method, by identifying the poles of the reflection coefficient with guided modes of the structure, described in [19]. This is a simplification of the real geometry, which includes the nanostructured back contact, with the assumption that the presence of the grating does not modify the mode structure very much. How reasonable this assumption is for the geometry under study (with nanoparticle heights of 40 nm) will be assessed by comparison to full field simulations of the nanostructured diode. We can then define the coupling condition, $R_{m,[pxpy],}$ as the wavelength at which, $\beta_m(\lambda) = G_{[px,py]}(\lambda)$, for each guided mode, m, and diffraction order, $[p_x p_y]$, combination.

How much of the light incident at the back surface is scattered into the diffraction orders depends on the grating under consideration and on the diffracted order: with the lowest orders having stronger scattering and the highest orders having weaker scattering from standard diffraction theory. The full diffraction efficiency is dependent on the refractive index contrast between the grating and the surrounding media as well as the details of the grating: the groove depth, geometry and fill factor. Plasmonic metal nanoparticle (MNP) based gratings can

#253156 Received 3 Nov 2015; revised 23 Dec 2015; accepted 3 Jan 2016; published 11 Jan 2016

support localised surface plasmons which can be very strongly scattering for relatively small MNP heights [27]. For MNP gratings, the diffraction efficiency is determined by the spectral overlap of the plasmonic scattering resonance of the MNPs with the diffraction orders of the grating [28,29]. If this is achieved, then the amount of light scattered at resonance depends on the normalized scattering cross-section (defined as the area over which the MNP scatters light divided by its cross-sectional area) and the surface coverage or density of the MNPs, F, as defined in Fig. 1(b). As a rule of thumb, the area over which the individual MNP interact with light should be larger than the unit cell of the grating to ensure that a significant fraction of the incident light is scattered.

We define the coupling efficiency as how much of the light scattered into a given diffraction order (DO) will be coupled into a given guided mode (GM) when the resonant coupling condition is fulfilled. When estimating the limits of light trapping in thin absorbers it is common to assume that the coupling efficiency is equal for all resonant coupling conditions (for example Stuart et al. [10] and Yu et al. [11]), which is equivalent to assuming the occupation of all available optical modes in the structure. For a bulk structure, this assumption leads to the well-known Lambertian limit [9]. However, in general this does not have to be true and the coupling efficiency can be different for different resonant coupling conditions.

The absorption enhancement provided by coupling to a given mode depends on the fraction of light dissipated in the mode that is usefully absorbed in the semiconductor. The energy dissipation of a given mode is determined by the material properties of the multi-layered substrate and the electric field profile of the mode across the film. The fraction of the total light absorbed that is absorbed in the active layer is calculated as:

$$P_m^{Frac} = \frac{P_{m,Active}}{P_{m,Total}}, \tag{1}$$

where $P_{m,j}$ is the energy dissipation in mode m, with an electric field profile E_m, integrated over the jth region of the multi-layer film:

$$P_{m,j} = \int_j 2\omega\varepsilon_0 \,\mathrm{Im}(\varepsilon_j)\left|\bar{E}_m\right|^2 dz. \tag{2}$$

3. FDTD simulations

To calculate the optical absorption in all parts of the multilayered geometry full-field, 3D optical simulations were performed with Lumerical FDTD software [30]. The simulation set up is shown schematically in Fig. 1(b), giving the position of the field monitors (black dashed lines), and the materials and thicknesses of the layers making up the structure. The periodic structure was represented by a single unit cell and illuminated by a normally incident plane wave. The simulation was terminated with perfectly matched layer boundary conditions perpendicular to the plane of incidence and periodic boundary conditions in the other dimensions. The nanoparticle portion of the grating was modeled as a hemi-ellipsoid with height, h = 40 nm and varying radii, r. Optical constants for glass and Ag were taken from the Lumerical materials database, based on data from Johnson and Christy [31]. A simplified, wavelength independent refractive index of $N = 1.7 + i*0.03$ was used for ITO, based on the results of ellipsometry measurements of ITO films on glass deposited in house. For the PbS CQD, the optical constants were calculated from the absorption spectra of representative PbS QDs in solution using the Kramers-Krönig relation, following the method described in [25].

#253156 Received 3 Nov 2015; revised 23 Dec 2015; accepted 3 Jan 2016; published 11 Jan 2016

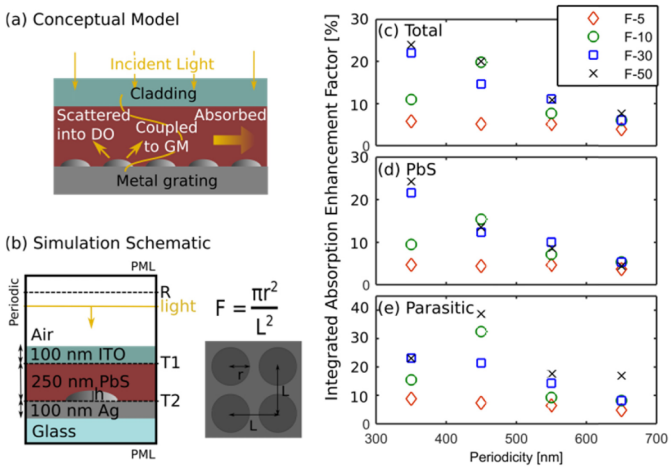

Fig. 1. (a) Schematic of the conceptual model showing the different processes occurring: light scattering into diffraction orders (DO); coupling to guided modes (GM); and absorption in the active layer. (b) Schematic of the simulation set up, illustrating the grating geometry and the definition of the surface coverage fractions, *F*. (c-e) Integrated absorption enhancement factor,F_{XEnh}, (as defined in the text below) calculated from FDTD simulations of the multilayer structure shown in part (b), and integrated over the wavelength range simulated ($400 < \lambda < 1100$ nm), for gratings with different periodicities, *L*, and surface coverage fractions, *F*. Data is given for (c) total absorption enhancement, (d) absorption enhancement in the PbS layer, and (e) enhancement of the parasitic absorption in the metal and ITO layers.

To calculate absorption in the nanoparticle portion of the grating, A_{MNP}, the absorbed power in the metal was integrated over the volume of the nanoparticle and normalized to the incident power. The electric field in 3D was monitored in a cubic volume enclosing the nanoparticle and the absorbed power per unit volume at point *p* was calculated using the Poynting's Theorem for dispersive media, which (for a non-magnetic material) with a wavelength dependent dielectric constant $\varepsilon(\omega)$, is given by: $\bar{P}_{Abs}(\bar{p},\omega)dV = \omega/2\,\Im m(\varepsilon(\omega))\left|\bar{E}(\bar{p},\omega)\right|^2$. $\bar{P}_{Abs}(\bar{p},\omega)dV$ was then integrated over the volume of the cube containing the metal, and normalized to the power injected into the simulation. By monitoring the power transmitted at both interfaces of the PbS layer, *T*1 and *T*2, and the power reflected by the structure, *R*, the total absorption, A_{Tot}, the absorption in the PbS, A_{PbS}, and the parasitic absorption, A_{Para}, can be calculated as follows:

$$A_{Tot} = 1 - R; \quad A_{PbS} = T1 - T2 - A_{MNP}; \quad A_{Para} = 1 - R - A_{PbS}; \ .$$

To quantify the change in absorption due to the nanostructuring of the rear electrode we calculate the absorption enhancement factor:

$$F_{XEnh} = \left(A_X^{Grating} - A_X^{Ref}\right) \Big/ A_X^{Ref},$$

where *X* represents where the absorption is occurring (*X* = *Tot, PbS* or *Para*, as defined above). This somewhat unconventional figure of merit is a measure of the fraction of the absorption in the PbS that is due to light trapping. This definition is useful as it avoids large, and largely meaningless, enhancement values which can occur when the semiconductor absorption is very low and $A_X^{Grating} / A_X^{Ref}$ is taken as the figure of merit.

#253156 Received 3 Nov 2015; revised 23 Dec 2015; accepted 3 Jan 2016; published 11 Jan 2016

4. Detailed analysis of resonant coupling

From our conceptual model, the periodicity, L, of the grating controls the resonant coupling with the guided modes of a given structure as well as the total diffraction efficiency through changes in the surface coverage fraction, F. We can fix F to compare different L values but then the radius, r, of the particle changes, which will also affect the scattering and parasitic absorption in the particles [27].

In order to compare different resonant coupling conditions we empirically determine the F values for which the full diffraction efficiency is relatively independent of r; this occurs when the particles are large and strongly scattering, with relatively broad resonances.

Figure 1(c)-1(e) shows the calculated integrated absorption enhancement factor in different parts of the multi-layered structure: 1(c) in the total volume, 1(d) in the PbS (i.e. the useful absorption enhancement), and 1(e) the parasitic absorption enhancement including losses in the ITO and metal grating. The integration is performed over the simulated spectrum (400 nm < λ < 1100 nm).

A low surface coverage of F = 5% results in very low absorption enhancements in all parts of the structure, with negligible dependence on L. This is attributed to the fact that the MNPs are too small (45 nm < r < 85 nm) and sparse to efficiently scatter and diffract, hence the absorption enhancement is low regardless of which coupling conditions are fulfilled. For larger values of F = 10 - 50%, the absorption enhancement in the CQD PbS is strongly dependent on L [Fig. 1(d)], and is relatively insensitive to F for a given periodicity (with the exception of F = 10%, L = 350 nm, r = 62 nm where the particle is still relatively small). Larger parasitic losses [Fig. 1(e)] are associated with higher F values, as expected due to the increase in the volume of metal in the structure, but these are offset by higher total absorption enhancements, i.e reduction in reflection [Fig. 1(c)]. Crucially, once the nanoparticles are sufficiently large to scatter strongly (85 nm < r < 250 nm), the absorption enhancement in the PbS is not sensitive to changes in the MNP size. In contrast, the enhancement in the PbS is strongly reduced with increasing periodicity, that is, when different resonant coupling conditions are fulfilled.

In this case, where the density and size of the nanoparticles is sufficienct to achieve strong scattering, it is not immediately clear why larger L values provide lower absorption enhancements as larger periodicities lead to more resonant coupling conditions in the wavelength range of interest. In order to investigate this further, we fix the surface coverage at F = 50%, and compare two slightly different multi-layer geometries. This allows us to compare different mode structures, following the work of Haug and colleagues [18]. Case 1 is the same as modelled in Fig. 1, with dimensions as shown in Fig. 1(b); while case 2 includes a thin ITO buffer layer between the grating and the PbS absorbing layer shown in the inset in Fig. 2(c). The dispersion relations of these two structures are similar with one important exception: in case 1 the lowest order transverse magnetic (TM0) mode is strongly localised to the metal|PbS interface and can be identified with a surface plasmon polariton (SPP) [4]; while in case 2 the SPP mode is localised on the metal|ITO interface.

Figures 2(a)-2(c) give absorption enhancement factor spectra plotted over a range of lattice vectors, G, for case 1 [2(a)], and case 2 [2(c)]. Green vertical lines show G[01] for each value of L. The resonant coupling conditions, $R_{m,[pxpy]}$, for the two lowest diffraction orders, ([$p_x p_y$] = [01] [11],), and for different guided modes, m, are superimposed on the plot. Dotted lines connect $R_{m,[pxpy]}$ for the transverse electric modes, (m = TE0,TE1, electric field perpendicular to the interface), while the transverse magnetic modes (m = TM0, TM1, electric field parallel to the interface) are connected by dashed lines.

While it is clear that absorption peaks in the spectra can be attributed to fulfilment of resonant coupling conditions, it is also clear that not all coupling conditions result in strongly enhanced absorption. Certain guided-mode|diffraction-order combinations lead to larger F_{AbsEnh} values. For both cases the strongest absorption enhancement occurs for coupling

#253156 Received 3 Nov 2015; revised 23 Dec 2015; accepted 3 Jan 2016; published 11 Jan 2016

between the TM0 mode and the lowest diffraction order, i.e $R_{TM0,[01]}$. Substantial absorption enhancement can also be attributed to coupling between higher order TM modes and diffraction orders: $R_{TM0,[11]}$, $R_{TM1,[01]}$ and $R_{TM1,[11]}$.

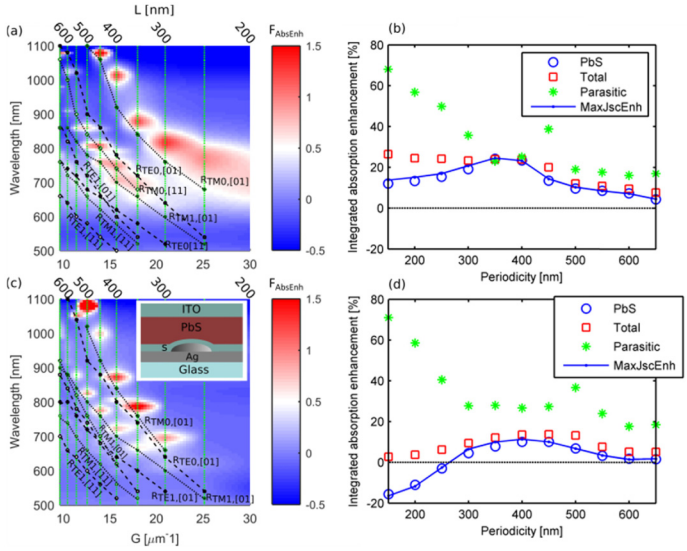

Fig. 2. (a) and (c) Absorption enhancement factors, F_{AbsEnh}, for different periodicities, L, and corresponding, reciprocal lattice vectors, G, calculated from FDTD simulations of the multilayer structure shown in Fig. 1(b) and in the insert in part Fig. 2(c), respectively. The surface coverage fraction is F = 50%. Simulations were performed for 200 nm < L < 650 nm in steps of 50 nm and the results were interpolated for clarity, without distorting the overall trends. Also plotted are the resonant coupling conditions, $R_{m,[pxpy]}$, for different guided modes: TE dashed lines, TM dotted lines. (b) and (d) Absorption enhancement factors from (a) and (b) respectively, integrated over the wavelength range simulated (400 < λ < 1100 nm). Data is given for absorption enhancement in the PbS layer, total absorption enhancement, enhancement of the parasitic absorption, as well as the maximum short circuit enhancement, which is calculated by convoluting A_{PbS} with the number of above bandgap photons in the solar spectrum.

There is generally good agreement between peaks in the spectra of the F_{AbsEnh} and the spectral positions of these $R_{m,[pxpy]}$: deviations between the two are attributed to the fact that the guided modes are calculated for a planar metal|semiconductor interface and do not account for the presence of the grating. Figure 2(b) and 2(d) shows the L dependence of integrated absorption enhancement factor in the total film (red squares), the PbS (blue circles), and the parasitic losses (green, stars) for 2(b) case 1, and 2(d) case 2, calculated from the data in parts 2(a) and 2(c) respectively. The estimated maximum short circuit current enhancement (MaxJscEnh, blue line) is also plotted, calculated by convoluting the absorption in the PbS with the solar spectrum (AM1.5g) and integrating over the simulated spectrum from 400 nm < λ < 1100 nm.

By comparing Figs. 2(a) and 2(b) we can see that the highest values of integrated absorption enhancements in the PbS for case 1 are for L = 350 nm and L = 400 nm, when $R_{TM0,[01]}$ occurs at wavelengths where light trapping is most effective, i.e. close to the exciton peak, in agreement with previously published work [4]. For L = 450 nm, $R_{TM0,[01]}$ is red-shifted to λ = 1050 nm where PbS is very weakly absorbing and light propagating in the mode will be dissipated mainly on the Ag side of the interface, resulting in a large increase in the parasitic absorption (also observed in Fig. 1(c)). For L > = 500 nm, $R_{TM0,[01]}$ occurs at λ > 1100 nm and hence does not lead to absorption increase in the PbS. In these cases the main contribution to the integrated absorption enhancement is due to $R_{TM0,[11]}$.

#253156 Received 3 Nov 2015; revised 23 Dec 2015; accepted 3 Jan 2016; published 11 Jan 2016

While the overall gains in useful absorption are lower in case 2 than those for a grating with no buffer layer, we find the same dependence on first order coupling to the TM0 mode from inspection of Figs. 2(c) and 2(d): the largest integrated absorption enhancement in the PbS is for L = 400 nm, where $R_{TM0,[01]}$ occurs at λ ~900 nm; and large parasitic losses occur when $R_{TM0,[01]}$ is red-shifted to λ ~1050 nm for L = 500 nm.

From this analysis it is clear that coupling to a specific mode, i.e. the TM0 mode, dominates the absorption enhancement in both cases and that the spectral position of $R_{TM0,[01]}$ is critical for providing large overall absorption enhancements. In order to understand why different coupling conditions result in different absorption gains we return to our conceptual model of light trapping. There are three factors that affect the absorption enhancement for a given resonant coupling condition: 1 - *the scattering and diffraction efficiency*; 2 - *the coupling efficiency between the diffraction order and the mode*; and 3- *the fraction of energy dissipated in the mode that is absorbed in the PbS,* P_m^{Frac}. To compare the relative importance of these effects, we identify different periodicities which exhibit clear absorption peaks at similar wavelengths, but that are attributed to different resonant coupling conditions.

Figures 3(a) and 3(b) shows the calculated absorption in the PbS film from selected simulations; with 3(a) L = 350, 450 and 500 nm for case 1 with no buffer layer; and 3(d) L = 400 and 450 nm for case 2 with a thin s = 50 nm buffer layer. Absorption peaks occur in all spectra at λ ~880 nm, due to different coupling conditions as labelled on the figure.

There are 2 important comparisons to be made: firstly between $R_{TM0,[pxpy]}$ with the same guided mode but different diffraction orders, as in case 1 [Fig. 3(a)] for L = 350 nm and L = 450 nm. Here, weaker diffraction into [11] order compared to the [01] order results in lower absorption at λ ~880 nm. The second comparison is between $R_{m,[01]}$ with the same diffraction order [01] but different guided modes: L = 350 nm and L = 500 nm. In this case there is negligible difference in scattering and diffraction from the grating due to the small variation in MNP sizes, as demonstrated in Fig. 1. In Fig. 3(a) we clearly see stronger enhancement for coupling to TM0 mode. In this case we conclude that larger absorption at λ ~880 nm for the L = 350 nm structure is due to a combination of differences in the fraction of light dissipated in the mode that is usefully absorbed in the semiconductor, P_m^{Frac}, and the coupling efficiency. Likewise a similar comparison can be made for case 2 in Fig. 3(b) between L = 400 nm and L = 450 nm, with $R_{TM0,[01]}$ and $R_{TE0,[01]}$ respectively . Again, the coupling to TE0 results in much lower absorption at λ ~880 nm when all other factors (scattering efficiency and wavelength dependent absorption coefficient of the material) are kept constant.

We now turn our attention to the details of light propagation and absorption in the guided modes. Calculated mode profiles are in given in Figs. 3(c) and 3(d) for the TM0 (red) and TE0 (blue) modes, in 3(c) for case 1 with no buffer layer, and in 3(d) for case 2 with s = 50 nm. The interfaces in the film are indicated by thin black lines and the edge of the nanoparticle portion of the grating is shown with a thick black line. The calculated, P_m^{Frac}, is shown in Fig. 3(e) for TE0 (blue squares) and TM0 (red, circles) modes, and for both cases: case 1 (filled markers), and case 2 (open markers).

For both cases the TM0 mode shows strong localisation at the metal interface, characteristic of an SPP mode. A consequence of this is that P_{TM0}^{Frac} [Fig. 3(e)] is strongly dependent on the absorption coefficients on both side of the interface [20,32], and is significantly reduced by the presence of the buffer. In contrast, P_{TE0}^{Frac} is relatively flat across the spectra and is similar for gratings with and without a buffer layer, consistent with the fact that the maximum of the mode profile is in the PbS and only slightly overlaps with the position of the buffer. From these results we would predict higher absorption enhancement due coupling to the TE mode in both cases with and without a buffer layer. Instead we see the opposite trend. It is clear from Figs. 3(c) and 3(d) that a key difference between propagation in the TE0 and TM0 mode is the spatial overlap of the mode with the grating: the TM0 mode is strongly localized to the interface and hence the position of the grating, while the TE0 mode overlaps only slightly. The fact that this results in higher absorption at $R_{TM0,[pxpy]}$ is analogous

#253156 Received 3 Nov 2015; revised 23 Dec 2015; accepted 3 Jan 2016; published 11 Jan 2016

to the case of a discrete MNP on a substrate: it has been shown that the spatial overlap of the near-field of the MNP with the substrate is critical for high coupling efficiency [32]. Another way of thinking about this is to consider that the electric field driving the plasmonic resonance in the MNPs of the grating is much stronger for the TM0 mode compare to TE0 mode: hence light is more strongly scattered and more light is coupled into the mode.

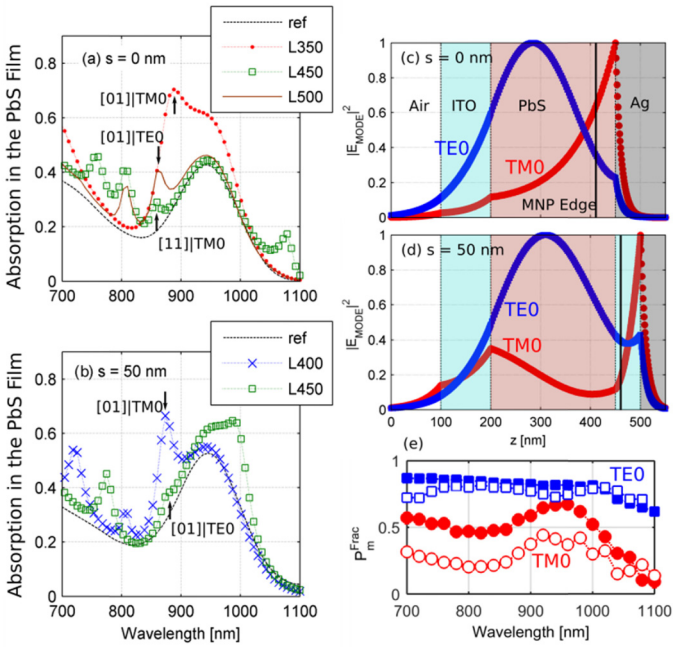

Fig. 3. (a,b) Calculated absorption spectra from simulations for (a) case 1 with no buffer layer (s = 0 nm), and (b) for case 2 with a buffer layer s = 50 nm. Data is shown for different grating parameters with F = 50% and L as shown in the legends. Resonant coupling conditions are indicated in the figures by labelled arrows. (c,d) Calculated mode profiles for the TM0 (red) and TE0 (blue) modes for (c) s = 0 nm and (d) s = 50 nm. (e) The fraction of light dissipated in the mode m that is absorbed in the PbS, P_m^{Frac}, for TE0 (blue squares) and TM0 (red, circles) and for s = 0 nm (filled markers), and s = 50 nm (open markers).

Finally, we observe that for similar coupling efficiency (i.e. mode overlap), fulfillment of the $R_{TM0,[01]}$ coupling condition leads to larger enhancement in case 1 than case 2 (L = 350 nm, Fig. 3(a), and L = 400 nm in Fig. 3(b)) due to the fact that P_{TM0}^{Frac} is higher for case 1 [Fig. 3(e)].

From the above discussion we conclude that the overlap of the spatial mode profile with the nanoparticle portion of the grating is an important indicator of the absorption enhancement in the PbS due to efficient mode coupling and strong excitation of the scattering mode.

5. Experimental verification of the results

Based on the insights gained above nanostructured back contacts were designed to provide light trapping for thin-film PbS CQD|ZnO hetero-junction photodiodes. The Au nanostructured back contacts were fabricated using standard electron beam lithography and lift-off processes, before the deposition of the semiconductor layers. Before semiconductor deposition, a thin layer of NiO of nominal thickness 5 nm was sputtered over the pre-prepared nanostructured electrodes, following the method of Mariano [33], as an electron blocking layer [34] and to improve adhesion. Both the ZnO and PbS nano crystals were synthesized in house and deposited from solution. The photodiodes were fabricated over the pre-patterned

#253156 Received 3 Nov 2015; revised 23 Dec 2015; accepted 3 Jan 2016; published 11 Jan 2016

contacts and grating structures using a layer-by-layer dip coating process. A partial ligand exchange of Oleic acid to Oleylamine was carried out before dip coating. To deposit a single layer, samples were dipped in the CQD solution (5 mg/ml in Hexane). We employed a two-step process to further cross link the QDs: the initial 5 layers were cross-linked by dipping for 3 seconds in 1,2-Ethanedithiol (EDT, 0.01% in Acetonitrile), while the remaining 25 layers employed tetrabutylammonium iodide as the ligand (TBAI, 10 mg/ml in MeOH). ZnO nanocrystals (40mg/ml in 5% MeOH in Chloroform) were deposited on top of the PbS layer by spin coating and the top ITO contact (110 nm) was then deposited by sputtering through a shadow mask.

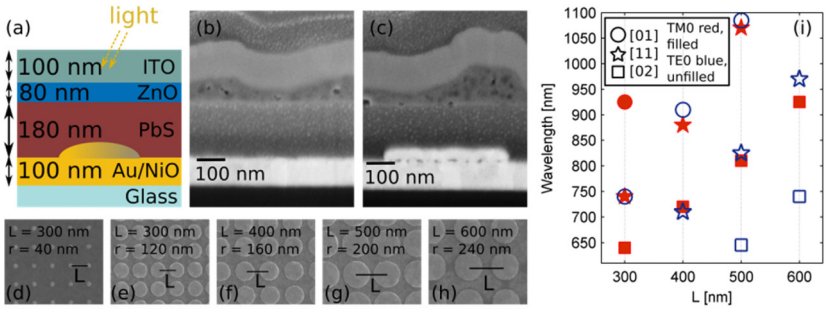

Fig. 4. (a) Schematic of the geometry of the PbS|ZnO photodiodes. (b,c) Cross sectional scanning electron microscope (SEM) images of the (b) planar and (c) nanostructured photodiodes (The layer visible on top of the ITO is the Pt deposited for milling in by focussed ion beam). (d-h) SEM images of the nanoparticle gratings. Scale given by the periodicity of the grating that is given for each image. (i) Predicted resonant coupling conditions, $R_{m,[pxpy],}$ for the two lowest order modes supported by the thin film devices, TM0 and TE0, and for the first three diffraction orders [01] [11], [02].

Figure 4(a) shows a schematic of the experimental photodiodes under study. Cross-sectional scanning electron microscope (SEM) images are given in Figs. 4(b) and 4(c) for planar and nanostructured devices respectively. The gratings are embedded in the PbS CQD film, resulting in a planar top interface, and similar active layer thicknesses for grating and reference photodiodes, estimated as t = 180 nm from the images shown. The ZnO layer is very rough, with thickness varying from 40 - 130 nm, and is conformally coated by the sputtered ITO layer. We would expect that incident light would be partially scattered by the roughness of the ITO/ZnO layer, which would spectrally broaden, and reduce the strength of the coupling peaks. Figures 4(d)-4(h) show SEM images of the nanoparticle gratings before deposition of the diode with periodicities as marked, with L = 300, 400, 500, 600 nm. The surface coverage fractions were F = 5% for the grating shown in 4(d); and F = 50% for the gratings shown in 4(e)-(h). The low F grating with L = 300 nm and r = 40 nm was fabricated as an additional reference; from integrated absorption enhancement data shown in Fig. 1(c) we do not expect it to provide efficient light trapping due to low scattering efficiency.

The spectral positions of the predicted resonant coupling conditions, $R_{m,[pxpy],}$ for the different grating periodicities are given in Fig. 4(i), for the two lowest order modes supported by the thin film devices, TM0 and TE0, and for the first three diffraction orders [01] [11], [02]. From Fig. 4(i), and insights gained from simulations above, we can predict that the L = 300 nm, r = 120 nm grating will produce large absorption gains at wavelengths close to the exciton peak of the PbS material, due to fulfillment of $R_{TM0,[01].}$ For larger L values our model predicts smaller absorption gains due to higher order diffractive coupling to the TM0 mode, and coupling to the TE0 mode.

Figure 5 shows representative EQE spectra of PbS|ZnO photodiodes with grating back contacts. In this work we employ the same contact geometry and measurement set up reported in [4]. The photocurrent was measured with a semiconductor parameter analyzer (Agilent,

#253156 Received 3 Nov 2015; revised 23 Dec 2015; accepted 3 Jan 2016; published 11 Jan 2016

B1500A). The diodes were illuminated with spectrally filtered and focused light (x20, NA 0.4) from a super continuous light source (NKT Photonics, SuperKExtreme EXW-4) in the wavelength range from 640 nm to 1100 nm. The active area under illumination was defined by the spot size with a diameter of 30 μm, as estimated using a knife edge measurement. For each grating, an adjacent planar area was measured as a reference. In order to isolate the contribution of increased absorption to the photocurrent enhancement we apply a small reverse bias of 500 mV during measurement, to improve the collection efficiency. This also mitigates another problem that we have previously reported: that nanostructured contacts can increase the collection efficiency in photodiode devices [4].

The calculated PbS absorption spectra from FDTD simulations of the experimental geometry are shown in adjacent graphs for comparison.

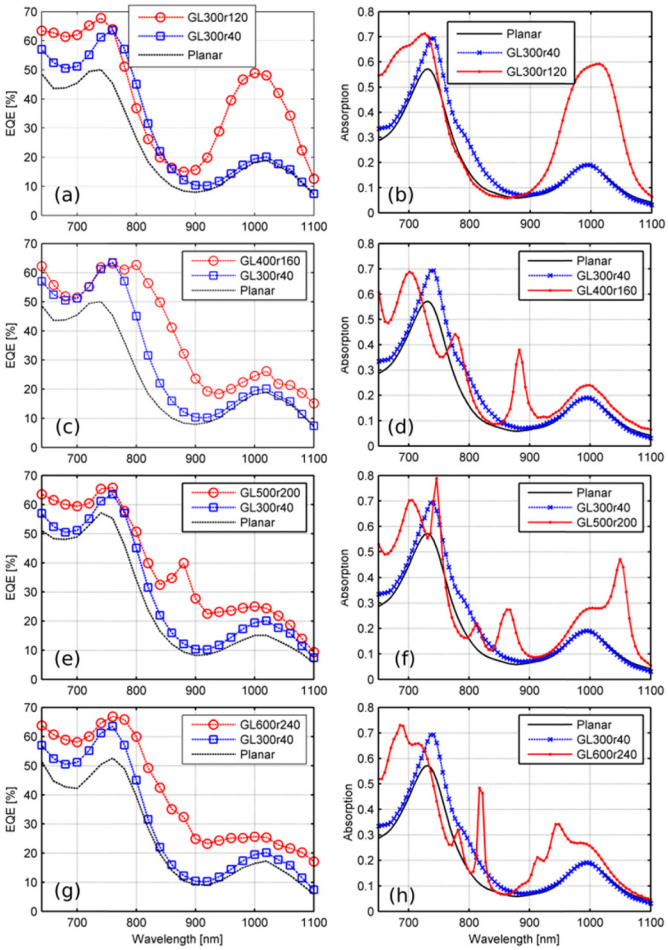

Fig. 5. (a,c,e,g) EQE of the PbS|ZnO photodiodes measured under a small reverse bias, V = –0.5 V, for different grating parameters, with F = 50% (red circles) and (a) L = 300 nm (GL300r120), (c) L = 400 nm (GL400r160), (e) L = 500 nm (GL500r200), (g) L = 600 nm (GL600r240). Data for planar references (Planar, black dashed lines), and the reference grating with F = 5%, L = 300 nm and r = 40 nm (GL300r40, blue squares) is also shown on each graph. (d,b,f,h) Calculated absorption in the PbS from FDTD simulations of the experimental geometry shown schematically in Fig. 4(a), with the same grating parameters and labelling conventions as in (a,c,e,g).

#253156 Received 3 Nov 2015; revised 23 Dec 2015; accepted 3 Jan 2016; published 11 Jan 2016

Data for planar references (black lines) and the reference grating (F = 5%, blue squares) are also plotted on each graph. To compare with the experimentally measured EQE in PbSZnO photodiodes, additional simulations of the experimental geometry were performed, as shown schematically in Fig. 4(a). The refractive index of Au was taken from the Lumerical materials database [30], based on data from Johnson and Christy [31].

The ZnO and ITO layers were modelled as a single, planar layer (i.e. without the roughness observed for the experimental samples in Figs. 4(b) and 4(c) with $N = 1.7 + i*0.03$. For historical reasons, the optical constants of the PbS used in the simulation study were slightly different than those of the experimental PbS: not only was a different ligand used experimentally but the spectral position of the excitonic peak had changed slightly. The optical constants were calculated using absorption spectra of QDs in solution that more closely matched the PbS QDs used in the experiment.

The agreement between the experimentally measured EQE under reverse bias and the calculated absorption in the PbS is generally good. Differences observed between the measured reference spectra represent the variation across the sample, which we attribute to local thickness differences from the spin coating process, and to spatial variation in film quality. For both modelled and measured cases the reference gratings, GL350r40, out-perform the planar references, due to near-field absorption enhancement provided by the small nanoparticles as demonstrated previously [4]. The peaks in measured EQE and calculated absorption occur at wavelengths approximately corresponding to the predicted coupling conditions, $R_{m,[pxpy],}$ in Fig. 4(i). As commented on above, the roughness of the ZnO/ITO layer will result in partial scattering of the incident light, in turn leading to deviation of the diffracted light from the calculated G, and hence variation in the coupling condition. The extent to which this effects the agreement between the measured and modelled spectra, with respect to the spectral position and strength of the observed peaks, depends on the details of the coupling condition for each case.

The broad peak at the exciton band (λ = 1000 nm) in the experimentally measured EQE spectrum of GL300r120 in Fig. 5(a) agrees very well with the modelled absorption spectra in Fig. 5(b). This is because the dispersion relation of the TM0 mode is relatively flat around the exciton peak; hence the peak is broad and is not sensitive to small changes in the coupling condition due to variations in incident angle. Conversely, the dispersion relations of the modes in the wavelength range 750 nm < λ < 900 nm have relatively steep gradients: any change in the coupling condition leads to a significant shift in the spectral position, width and strength of the resonance. For this reason, the sharp peaks calculated between wavelengths 750 nm < λ < 900 nm for GL400r160 in Fig. 5(d) and GL600r240 in Fig. 5(h) are observed to shift wavelength slightly, reduce in strength, and broaden significantly in the experimental spectra. The missing long wavelength peak at λ = 1075 nm for the GL500r200 grating in Fig. 5(e) is likely due to an overestimation of the PbS absorption coefficient in the simulations at wavelengths beyond the exciton peak.

The key result from Fig. 5 is that the largest EQE enhancement occurs for the GL350r120 grating, due to the $R_{TM0,[01],}$ as predicted by the conceptual model. Comparing Fig. 5(a) and 5(c): we achieve a measured EQE enhancement of up to 2.5 times the reference case at the exciton peak (λ = 1000 nm) for the optimised coupling to the TM0, compared to an increase of just 25% at the same wavelength for coupling to the TE0 mode. We can conclude that our simple conceptual model is useful in predicting and optimizing the light trapping potential of grating structures in multilayer geometries.

6. Conclusion

We have demonstrated that understanding light trapping with scattering structures in terms of the fulfillment of specific resonant coupling conditions, scattering/diffraction efficiency, and coupling efficiencies can inform the design of these structures in a simple and intuitive manner; without the need to resort to computationally expensive simulation sweeps. This

#253156 Received 3 Nov 2015; revised 23 Dec 2015; accepted 3 Jan 2016; published 11 Jan 2016

method is fully compatible with other material systems and device architectures, relying only on knowledge of the guided modes supported by the geometry.

A key result of this work is the importance of the mode profile which determines not only the fraction of light usefully absorbed, but also the excitation of, and coupling to, the scattering resonance. Here we show that while SPP modes have higher parasitic losses than the fundamental photonic mode, resonant coupling to the SPP mode results in larger absorption in the film due to larger overlap with the grating.

In the geometry presented here, targeting the SPP mode at the exciton peak leads to both the largest enhancement at a given wavelength and the largest overall enhancement. This is partly because the dispersion relation of the SPP mode is very flat at these wavelengths, leading to broad resonances. In general there will be different optimisations for targeting narrow-band versus broadband enhancement.

While we have focused on periodic gratings in order to elucidate the physical processes occurring during resonant coupling, we note that periodic structures are not necessarily optimal for maximising broadband light absorption; of particular interest for PV applications. Both Pala [15] and Martins [17]demonstrate that quasi-periodic structures allow flexibility to provide more spatial frequencies for coupling at the desired wavelengths. In general, the principles of the model presented here can inform the design of quasi-periodic and random systems as well as periodic arrays. If the spatial frequencies or angular scattering distribution is known then the resonant coupling conditions can be estimated, and the importance of the mode profile in maximizing enhancement holds.

Acknowledgments

This research has been supported at ICFO by Fundacio´ Privada Cellex Barcelona and the European Commission's Seventh Framework Programme (FP7) for Research under contract PIRG06-GA-2009-256355 and the Ministerio de Ciencia e Innovacion under contract number TEC2011-24744. FJB acknowledges the support of the Marie Curie postdoctoral fellowship PECQDPV, under the FP7-people-2011-IIF program, while at ICFO; and the FERL Fellowship while at ANU. The authors would like to thank M. Mariano for NiO sputtering and M. Lundeberg for wire bonding of samples, and N. Lal for comments on the manuscript.

#253156 Received 3 Nov 2015; revised 23 Dec 2015; accepted 3 Jan 2016; published 11 Jan 2016